Finite mass transfer effects in cavitation modelling

Schenke, Sören; van Terwisga, Thomas

Publication date
2016

Document Version
Accepted author manuscript

Published in
Proceedings of the 19th Numerical Towing Tank Symposium (NuTTS 2016)

Finite Mass Transfer Effects in Cavitation Modelling

Sören Schenke* **and Tom J.C. van Terwisga*†**
*Delft University of Technology, Delft/The Netherlands, †Maritime Research Institute Netherlands, Wageningen/The Netherlands
s.schenke@tudelft.nl

1 Introduction

One of the key aspects classifying the various approaches in numerical simulation of cavitating flows is the equilibrium flow assumption. It states that internal processes in the flow always occur instantaneously compared to the time scale of the flow (s. Sezal (2009)). As a consequence, the density-pressure trajectory in a barotropic flow may follow a unique curve. Contrary to the equilibrium flow assumption, one may assume that the time to achieve a new state is governed by the magnitude of a finite mass transfer source term in a volume fraction transport equation (s. Asnaghi et al. (2015)). In this case, the set of possible density-pressure states is not predefined, but strongly depends on the rate at which pressure changes. Although it has been pointed out by Koukouvinis and Gavaises (2015) that the equilibrium assumption for a barotropic flow would theoretically be mimicked by the mass transfer model if the finite transfer rate tended to infinity, the model parameters triggering the finite transfer rate are generally considered as empirical (s. Frikha et al. (2008)).
In this paper, effects of the finite mass transfer rate with special focus on condensation will be studied in detail. First, a cavity collapse will be considered to demonstrate how the finite transfer source term must be modified to satisfy the equilibrium flow assumption. Second, a single bubble collapse is studied numerically and effects of the finite mass transfer rate will be discussed.

2 Finite Mass Transfer Approach and Equilibrium Flow Assumption

Following Asnaghi et al. (2015), the finite mass transfer rate is expressed as a source term in the transport equation for the liquid volume fraction γ, where u is the velocity of the mixture flow, ρ_l the liquid density and C a constant to adjust the magnitude of the source term:

$$\frac{\partial \gamma}{\partial t} + \nabla \cdot (\gamma u) = \frac{C\psi(p,\gamma)}{\rho_l} \tag{1}$$

The density is perceived as a mixture quantity, varying according to the volume fraction γ, such that $\rho = \gamma\rho_l + (1-\gamma)\rho_v$, where ρ_v denotes the vapour density. Substituting first the mixture density and then the volume fraction transport equation (1) into the mass conservation equation

$$\frac{\partial \rho}{\partial t} + \nabla \cdot (\rho u) = 0, \tag{2}$$

and further taking into account that the individual phase densities are considered as constant values, yields a local velocity divergence (s. Asnaghi et al. (2015))

$$\nabla \cdot u = S_{\text{fin}} = kC\psi(p,\gamma), \qquad \text{where} \qquad k = \frac{1}{\rho_l} - \frac{1}{\rho_v}. \tag{3}$$

To modify the finite source term S_{fin} in a way that it satisfies the equilibrium flow assumption, the collapse of a spherical cavity is considered and C is now associated with a condensation constant C_c. The reason why condensation is addressed in particular, is the underlying assumption that the motion of a condensation front is driven by pressure gradients, similar to the motion of a bubble interface obtained from the Rayleigh-Plesset equation (s. Franc and Michel (2004)). The local condensation time in an infinitesimal small control volume dV_C as illustrated in Fig. 1 must then be in line with the accelerating condensation front to achieve an equilibrium state at any instance in time. Applying the Gauss-theorem to the control volume dV_C yields

$$dV_C \nabla \cdot u = u_e dA_e - u_w dA_w, \tag{4}$$

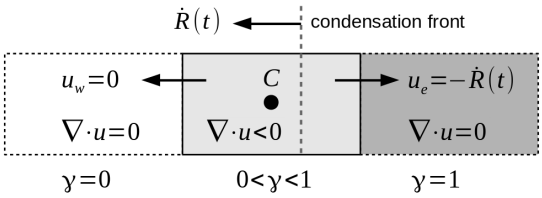

Fig. 1: Condensing control volume

where u_e and u_w denote the in- and outflow velocity of the control volume, presuming that the normal vector of the condensation front is perpendicular to the corresponding in- and outflow surface given by A_e and A_w. As the condensation front passes the control volume with a speed $\dot{R}(t)$, its density increases at a rate governed by $\dot{R}(t)$. This is reflected by the boundary conditions $u_e = -\dot{R}(t)$ and $u_w = 0$, which gives

$$dV_C \nabla \cdot u = -\dot{R}(t)\, dA_e \qquad \Rightarrow \qquad \nabla \cdot u = -\frac{\dot{R}(t)}{dx}. \tag{5}$$

To achieve an equilibrium state, the control volume must be fully condensed within the time T that it takes for the interface to pass the control volume length dx. Thus, the control volume is fully occupied by vapour at time instance $t = 0$, fully condensed at time instance $t = T$ and the relation between length dx and local condensation time T associated with the control volume is given by

$$\int_0^T \dot{R}(t)\ \mathrm{d}t = dx. \tag{6}$$

From Eq. (6) it follows that the source term must be time dependent to satisfy the equilibrium assumption. Substituting the velocity divergence by a time dependent source $S(t)$ yields $S(t) = -\dot{R}(t)/dx$. Integration and substitution of Eq. (6) gives

$$\int_0^T S(t)\ \mathrm{d}t = \frac{1}{dx}\int_0^T \dot{R}(t)\ \mathrm{d}t = -1. \tag{7}$$

Eq. (7) imposes a restriction on the time integral of the source term $S(t)$ over the local condensation time T. The time integral is now replaced by an integral over pressure by multiplying the finite source term $S_{\mathrm{fin}} = kC_{\mathrm{c}}\psi(p,\gamma)$ with the pressure time derivative $\partial p/\partial t$, such that

$$\int_0^T S(t)\ \mathrm{d}t = kC_{\mathrm{c}}\int_0^T \psi(p,\gamma)\left(\frac{\partial p}{\partial t}\right)\mathrm{d}t = kC_{\mathrm{c}}\int_{p(0)}^{p(T)} \psi(p,\gamma)\ \mathrm{d}p = -1. \tag{8}$$

The thermodynamic states corresponding to time instances $t = 0$ and $t = T$ are given by vapour pressure $p(0) = p_v$ and condensation pressure $p(T) = p_{\mathrm{c}}$, respectively. Further presuming that the interim states are given by a barotropic equation of state $\rho(p)$, the term $\psi(p,\gamma)$ can be associated with a local compressibility law for $\partial\rho/\partial p$ and we get

$$\int_{p(0)}^{p(T)} \psi(p,\gamma)\ \mathrm{d}p = \int_{p_v}^{p_c}\left(\frac{\partial\rho}{\partial p}\right)\mathrm{d}p = \int_{\rho(p_v)}^{\rho(p_{\mathrm{c}})}\mathrm{d}\rho = \rho_l - \rho_v. \tag{9}$$

Substituting Eq. (9) into Eq. (8), then solving Eq. (8) for C_{c} and substituting back into the time dependent source term $S(t) = kC_{\mathrm{c}}\psi(p,\gamma)\,\partial p/\partial t$ yields

$$\nabla \cdot u = S(t) = -\frac{\psi(p,\gamma)}{\rho_l - \rho_v}\frac{\partial p}{\partial t}. \tag{10}$$

Eq. (10) represents the modified source term that satisfies the equilibrium flow assumption. It should be noted that $\psi(p,\gamma)$ may still scale with another constant such that Eq. (9) is satisfied.
To study the effect of finite mass transfer on condensation and evaporation, the ρ-p trajectory at an

isolated point in space will be determined. To further isolate the effect of mass transfer, it is supposed that the density gradient is zero. Thus, the temporal density change at that point is only a result of velocity divergence or mass transfer, respectively. In this case, the mass conservation Eq. (2) simplifies to

$$\nabla \cdot u = -\frac{1}{\rho}\frac{\partial \rho}{\partial t}. \tag{11}$$

Following the considerations above, the equilibrium flow approach basically distinguishes from the finite mass transfer approach by the factor $\partial p/\partial t$ (s. Eq. (12)). To simplify the comparison, both the finite and the equilibrium source term is multiplied with the same condensation/evaporation constant $C_{\mathrm{c,v}} = 1$. This means for the equilibrium approach that the pressure p_c, at which full condensation is achieved, is not predefined as in Eq. (9) but a result of the magnitude of C_c.

$$-\frac{1}{\rho}\frac{\partial \rho}{\partial t} = \begin{cases} kC_{\mathrm{c,v}}\psi\left(p,\gamma\right) & \text{finite mass transfer} \\ kC_{\mathrm{c,v}}\psi\left(p,\gamma\right)\frac{\partial p}{\partial t} & \text{equilibrium flow} \end{cases} \tag{12}$$

In Eq. (12), constant $C_{\mathrm{c,v}}$ is considered as dimensionless in both cases and the dimension of $\psi\left(p,\gamma\right)$ is adjusted accordingly. Eq. (12) is solved for ρ numerically by employing a backward Euler step $\partial\rho/\partial t = \left(\rho^t - \rho^{t-1}\right)/\Delta t$. Employing the cavitation model by Merkle et al. (1998), the finite mass transfer rate is written as a superposition of a condensation and an evaporation term as follows:

$$C_{\mathrm{c,v}}\psi\left(p,\gamma\right) = \frac{1}{\rho}\left[\left(1-\gamma\right)C_c\max\left(p-p_v,0\right) + \gamma C_v\min\left(p-p_v,0\right)\right] \tag{13}$$

The volume fraction γ is updated explicitly such that $\gamma^{t-1} = \left(\rho^{t-1} - \rho_v\right)/\left(\rho_l - \rho_v\right)$. The pressure growth rate $dp/dt = \dot{p}$ is assumed as constant, such that $p^t = p^{t-1} + \dot{p}\Delta t$. Convergence with respect to the time step size was ensured by systematic variation of Δt, where $\Delta t = 10^{-4}$ s was found to be sufficiently small. For both condensation and evaporation, the starting pressure is $p_v = 2340$ Pa. The corresponding starting densities are $\rho_v = 0.02\ \mathrm{kgm^{-3}}$ and $\rho_l = 1000\ \mathrm{kgm^{-3}}$, respectively.
Fig. 2 left illustrates the impact of the pressure growth rate $\dot{p}$, which tends to stretch out the condensation/evaporation curves for increasing values in case of finite mass transfer. This is explained by the circumstance that the density growth/decay tends to lack behind when the pressure growth rate is increased for the same finite mass transfer rate. For the equilibrium flow approach, however, all the state curves merge to one single curve associated with a pressure growth/decay rate of $1.0\ \mathrm{Pas^{-1}}$ in the finite mass transfer case.

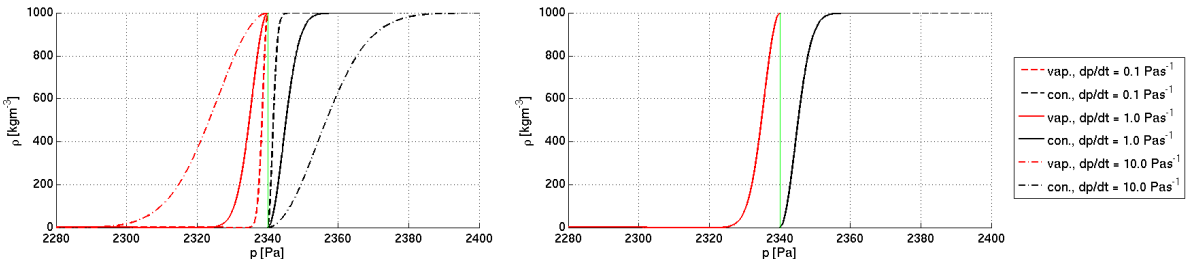

Fig. 2: ρ-p trajectories for the finite mass transfer approach (left) and the equilibrium flow assumption (right)

3 Single Bubble Collapse - Effect of Finite Mass Transfer Rate on Flow Dynamics

To further investigate the impact of the finite mass transfer rate on the flow dynamics, the collapse of a single bubble is studied numerically, using the OpenFOAM solver interPhaseChangeFOAM. The Merkle model as represented by Eq. (13) is employed and only the Euler equations are solved. Again, liquid and vapour density are assumed to be $\rho_l = 1000\ \mathrm{kgm^{-3}}$ and $\rho_v = 0.02\ \mathrm{kgm^{-3}}$. The initial bubble radius is

$R_0 = 0.4$ mm and the bubble and its vicinity is embedded in a uniform polar grid with a resolution of 50 cells per mm in radial direction and 50 cells per $\pi/2$ rad in circumferential direction. Only one cell layer of one eight of the domain is simulated, applying corresponding symmetry and wedge boundary conditions as indicated in Fig. 3. The far field boundary is located at 0.5 m from the bubble centre, where the fixed value condition $p_\infty = 10^5$ Pa and zero gradient conditions for liquid volume fraction and velocity are applied. The initial liquid volume fraction is set to 0 inside the bubble and 1 outside the bubble. The initial pressure field satisfies the Laplace equation, which gives (s. Franc and Michel (2004))

$$\frac{p(r)}{\rho} + \frac{1}{2}\frac{R^4\dot{R}^2}{r^4} - \frac{1}{r}\left(2R\dot{R}^2 + R^2\ddot{R}\right) = \frac{p_\infty}{\rho}. \tag{14}$$

In Eq. (14), r is the radial coordinate and R denotes the location of the bubble interface. Applying the initial conditions $\dot{R}(t=0) = 0$ and $p(r=R_0) = p_v$ yields $\ddot{R} = (p_v - p_\infty)/(\rho R_0)$. Further assuming vapour pressure p_v inside the bubble yields the initial pressure field:

$$p(r) = \begin{cases} p_v & \text{if} \quad r \le R_0 \\ p_\infty + \frac{R_0}{r}(p_v - p_\infty) & \text{if} \quad r > R_0 \end{cases} \tag{15}$$

As a reference, the characteristic Rayleigh collapse time τ is obtained from numerical integration of the analytical solution for the bubble interface velocity derived from the Rayleigh-Plesset equation (s. Franc and Michel (2004))

$$\frac{dR}{dt} = -\sqrt{\frac{2}{3}\frac{p_\infty - p_v}{\rho}\left(\frac{R_0^3}{R^3} - 1\right)}, \tag{16}$$

which gives $\tau = 3.6933 \cdot 10^{-5}$ s. The integration was initialised with a bubble radius of $R_0 = 0.399999$ mm and forwarded with $R^t = R^{t-1} + \dot{R}\Delta t$, where $\Delta t = 10^{-10}$ s. The dimensionless radial pressure distribution is then given by (s. Franc and Michel (2004))

$$\Pi(r,t) = \frac{p(r,t) - p_\infty}{p_\infty - p_v} = \frac{R}{3r}\left[\frac{R_0^3}{R^3} - 4\right] - \frac{R^4}{3r^4}\left[\frac{R_0^3}{R^3} - 1\right]. \tag{17}$$

The evolution of the bubble radius over time (s. Fig. 4), the pressure wave moving towards the bubble

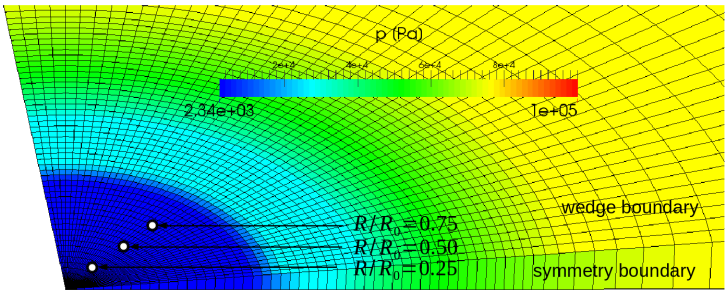

Fig. 3: Initial pressure field

centre with the bubble interface (s. Fig. 5) and the ρ-p trajectory (s. Fig. 6) at three different observation points indicated in Fig. 3 are of particular interest. The study is carried out for three different condensation rates $C_c = 10; 100; 1000$ with a time step size of $\Delta t = 5 \cdot 10^{-8}$ s. During the collapse, the initially sharp bubble interface is subjected to diffusion. The bubble radius is therefore estimated by computing the equivalent radius of a bubble that contains the same amount of vapour but which is fully occupied by vapour.

Concerning the evolution of the bubble radius in Fig. 4, a good agreement is achieved with the evolution predicted by the quasi analytical Rayleigh-Plesset equation (analytical RP). The slight overestimation is least pronounced for the medium condensation rate $C_c = 100$. For the smallest rate $C_c = 10$, however,

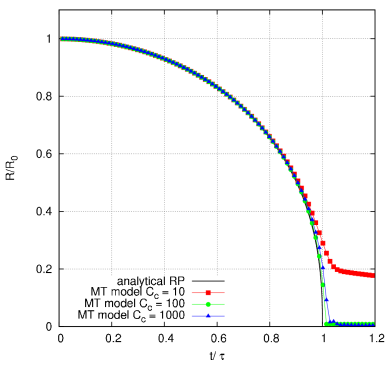

Fig. 4: Bubble radius evolution

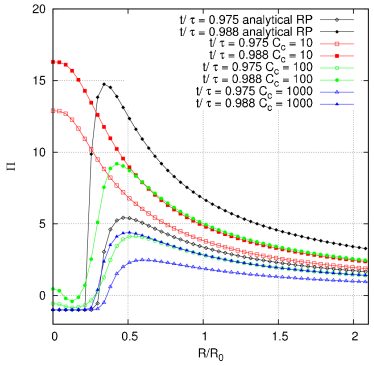

Fig. 5: Radial p-distribution

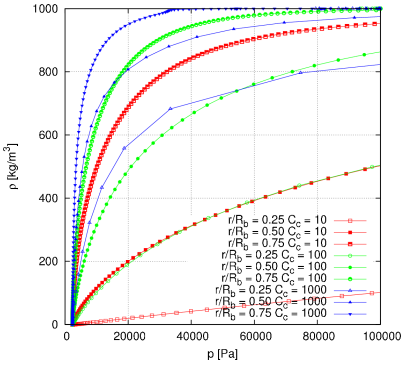

Fig. 6: ρ-p trajectories

the bubble radius evolution undergoes a sudden deceleration close to the final collapse stage. Concerning the radial pressure distribution, which is evaluated at two different time instances close to the final collapse stage, it is striking that the bubble interior pressure slightly increases above vapour pressure for the medium condensation rate $C_c = 100$, and significantly increases for the smallest condensation rate $C_c = 10$. Only the largest condensation rate $C_c = 1000$ preserves vapour pressure at the considered time instances. The steepness of the ρ-p trajectories increases with increasing condensation rate and decreases as the bubble centre is approached, where pressure changes more rapidly. This confirms the observations from Section 2. In addition, the following effects of finite mass transfer rate on the flow dynamics are identified.

Effects of finite mass transfer rate on the flow dynamics: It is recalled from Section 2 that the mass transfer rate should ideally be just large enough to prevent mass flux through the interface at any time instance. This can only be achieved by satisfying the equilibrium flow assumption, which requires a time dependent source term. Due to the neglect of time dependencies in the mass transfer term, the transfer rate is either too small or too large compared to the ideal situation and can only be correct at one instance in time. Based on that, two different mechanisms driving the flow towards the centre are identified. The major contribution results from the global pressure gradients, causing an inertia driven flow, which is observed in the analytical Rayleigh-Plesset model (s. Franc and Michel (2004)) in a similar way. In addition to that, the velocity divergence at the condensing interface is a secondary local driver. With the finite condensation rate being too small on the one hand, the inertia driven flow passes the condensing interface ($u_w > 0$ in Fig. 1). The flow then focuses to the centre quicker than the condensation front. Due to the symmetry of the flow, a stagnation point forms at the centre, explaining the pressure increase inside the bubble. With the condensation rate being too large on the other hand, the condensation time T associated with a local control volume tends to be smaller than the time that it takes for the inertia driven flow to pass the length dx of the control volume. However, the condensation front can not arbitrarily move ahead of the inertia driven flow, because the condensation rate also depends on the local pressure rise which goes along with the inertia driven flow. These two situations are further illustrated by Fig. 7 to 10.

A secondary velocity peak at the interface due to the strong velocity divergence is clearly observed in

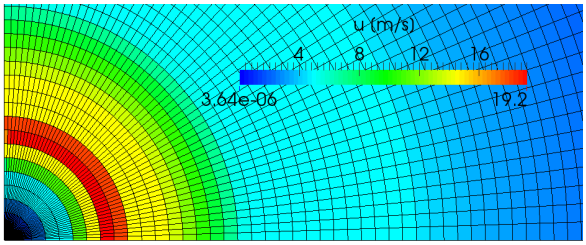

Fig. 7: Velocity magnitude for $C_c = 100$ at time instance $t/\tau = 0.8123$

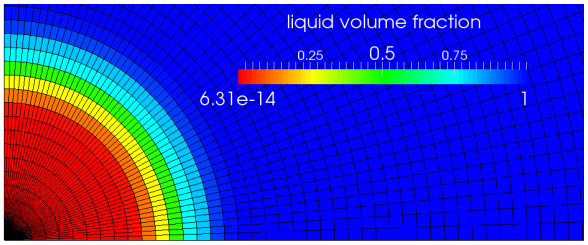

Fig. 8: Volume fraction for $C_c = 100$ at time instance $t/\tau = 0.8123$

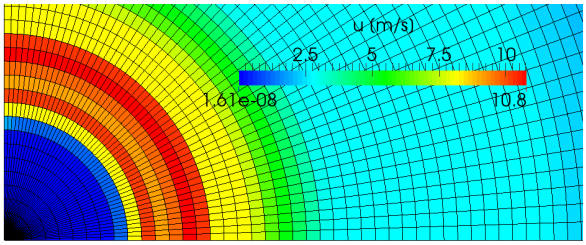

Fig. 9: Velocity magnitude for $C_c = 1000$ at time instance $t/\tau = 0.8123$

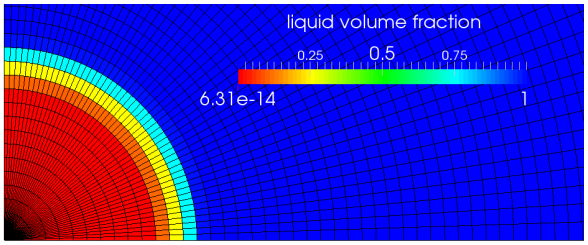

Fig. 10: Volume fraction for $C_c = 1000$ at time instance $t/\tau = 0.8123$

Fig. 9, which depicts the instantaneous velocity distribution at $t/\tau = 0.8123$ for $C_c = 1000$. Taking the instantaneous volume fraction in Fig. 10 into account, it appears that some mass flux has already passed the condensation front. However, this effect is much more pronounced in Fig. 7, which depicts the instantaneous velocity field for $C_c = 100$. The secondary velocity peak is not observed in this case and the interface itself appears to be more diffusive compared to the larger condensation rate. The misalignment of the two flow drivers when violating the equilibrium is likely one of the reasons for different predictions of the radial pressure distributions depending on the condensation rate (s. Fig. 5).

4 Conclusion

It has been demonstrated that the mass transfer approach satisfies the equilibrium flow assumption during a cavity collapse if the pressure time derivative $\partial p/\partial t$ is included in the source term of the volume fraction transport equation (s. Eq. (10)). Two different mechanisms driving the flow during the collapse have been identified. The first driver results from pressure gradients, causing an inertia driven flow and focusing it towards the cavity centre. The second driver results from the local velocity divergence at locations where the condensation source term is active, causing a local mass flux into the condensation front. The coupling of the condensation source term with the pressure time derivative establishes a dynamic equilibrium of the two drivers, such that the acceleration of the condensation front is in line with the inertia driven flow. The neglect of the pressure time derivative in the condensation source term results in a decoupling of the two mechanisms mentioned above. An equilibrium flow can still be simulated by applying very large finite mass transfer rates (s. Koukouvinis and Gavaises (2015)), thereby preventing mass flux through the condensation interface. However, the formation of a secondary velocity peak associated with the tendency of the condensation front to move ahead of the inertia driven flow, is likely to affect the pressure dynamics.

References

A. Asnaghi, A. Feymark and R.E. Bensow (2015). Numerical simulation of cavitating flows using OpenFOAM. Proceedings of NuTTS 2015, Cortona, Italy.

J.-P. Franc and J.-M. Michel (eds.) (2004). *Fundamentals Of Cavitation.* Kluwer Academic Publishers.

S. Frikha, O. Coutier-Delgosha, and J.A. Astolfi (2008). Influence of the cavitation model on the simulation of cloud cavitation on 2D foil section. *International Journal of Rotating Machinery*, vol. 2008.

P. Koukouvinis and M. Gavaises (2015). Simulation of throttle flow with two phase and single phase homogenous equilibrium model. Proceedings of CAV 2015, Lausanne, Switzerland.

C.L. Merkle, J.Z. Feng and P.E.O. Buelow (1998). Computational modeling of the dynamics of sheet cavitation. Proceedings of CAV 1998, Grenoble, France.

I.H. Sezal (2009). *Compressible Dynamics Of Cavitating 3-D Multi-Phase Flows.* Dissertation, Technische Universität München.